GRANDMA observations of ZTF/*Fink* transients during summer 2021

V. Aivazyan,[1,2] M. Almualla,[3] S. Antier ,[4,5,6] A. Baransky,[7] K. Barynova,[8] S. Basa,[9] F. Bayard,[10]
S. Beradze,[1,2] D. Berezin,[11] M. Blazek ,[12] D. Boutigny,[13] D. Boust,[14,15] E. Broens,[16,17] O. Burkhonov,[18]
A. Cailleau,[19] N. Christensen,[4] D. Cejudo,[20] A. Coleiro,[6] M. W. Coughlin ,[21] D. Datashvili,[1,2]
T. Dietrich,[22,23] F. Dolon,[24] J.-G. Ducoin,[25,26] P.-A. Duverne,[25] G. Marchal-Duval,[25] C. Galdies,[27,28]
L. Granier,[29] V. Godunova,[11] P. Gokuldass,[30] H. B. Eggenstein,[31] M. Freeberg,[32] P. Hello,[25]
R. Inasaridze,[1,2] E. E. O. Ishida,[33] P. Jaquiery,[34] D. A. Kann,[12] G. Kapanadze,[1,2] S. Karpov,[35] R.
W. Kiendrebeogo,[4,36] A. Klotz,[37,38] R. Kneip,[39] N. Kochiashvili,[1] W. Kou,[40] F. Kugel,[14] C. Lachaud,[6]
S. Leonini,[41] A. Leroy,[42,43] N. Leroy,[25] A. Le Van Su,[24] D. Marchais,[44] M. Mašek,[35] T. Midavaine,[6]
A. Möller,[33,45] D. Morris,[30] R. Natsvlishvili,[1] F. Navarete,[46] K. Noysena,[47] S. Nissanke,[5] K. Noonan,[48]
N. B. Orange,[48] J. Peloton,[25] A. Popowicz,[49] T. Pradier,[50] M. Prouza,[35] G. Raaijmakers,[5] Y. Rajabov,[18]
M. Richmond,[51] Ya. Romanyuk,[52] L. Rousselot,[53] T. Sadibekova,[18,54] M. Serrau,[14] O. Sokoliuk,[7,52]
X. Song,[40] A. Simon,[55,56] C. Stachie,[4] A. Taylor,[57,58,59] Y. Tillayev,[18,60] D. Turpin ,[54]★
M. Vardosanidze,[1,2] J. Vlieghe,[25] I. Tosta e Melo,[61] X. F. Wang[40,62] and J. Zhu[40]

Affiliations are listed at the end of the paper

ABSTRACT

We present our follow-up observations with GRANDMA of transient sources revealed by the Zwicky Transient Facility (ZTF). Over a period of six months, all ZTF alerts were examined in real time by a dedicated science module implemented in the *Fink* broker, which will be used in filtering of transients discovered by the Vera C. Rubin Observatory. In this article, we present three selection methods to identify kilonova candidates. Out of more than 35 million alerts, a hundred sources have passed our selection criteria. Six were then followed-up by GRANDMA (by both professional and amateur astronomers). The majority were finally classified either as asteroids or as supernovae events. We mobilized 37 telescopes, bringing together a large sample of images, taken under various conditions and quality. To complement the orphan kilonova candidates, we included three additional supernovae alerts to conduct further observations during summer 2021. We demonstrate the importance of the amateur astronomer community that contributed images for scientific analyses of new sources discovered in a magnitude range $r' = 17 - 19$ mag. We based our rapid kilonova classification on the decay rate of the optical source that should exceed 0.3 mag d^{-1}. GRANDMA's follow-up determined the fading rate within 1.5 ± 1.2 d post-discovery, without waiting for further observations from ZTF. No confirmed kilonovae were discovered during our observing campaign. This work will be continued in the coming months in the view of preparing for kilonova searches in the next gravitational-wave observing run O4.

Key words: gravitational waves – methods: data analysis – neutron star mergers.

1 INTRODUCTION

The landmark detection of GW170817 by LIGO and Virgo (Abbott et al. 2017a), GRB 170817A by Fermi-GBM (Goldstein et al. 2017) and INTEGRAL (Savchenko et al. 2017), and the subsequent accompanying host of electromagnetic signatures (Abbott et al. 2017b) solidified the long predicted connection of binary neutron star mergers (BNS) to short gamma-ray bursts (sGRBs; e.g. Alexander et al. 2017; Haggard et al. 2017; Hallinan et al. 2017), and optical/infrared transients called kilonovae (KNe; e.g. Arcavi et al.

2017; Andreoni et al. 2017; Hu et al. 2017). Signatures of KNe also exist in some sGRBs (e.g. Berger, Fong & Chornock 2013; Tanvir et al. 2013), and efforts to obtain a full characterization of their emission remain a major priority in Astrophysics. In particular, KN emission is uniquely suited to better constrain the neutron star equation of state (EoS; e.g. Bauswein et al. 2017; Margalit & Metzger 2017; Coughlin et al. 2018; Coughlin et al. 2019; Coughlin et al. 2020c), the Hubble constant (e.g. Abbott et al. 2017a; Hotokezaka et al. 2019; Coughlin et al. 2020a, b; Dietrich et al. 2020) and the abundancies of r-process nucleosynthesis (e.g. Chornock et al. 2017; Coulter et al. 2017; Cowperthwaite et al. 2017).

To address outstanding questions related to KNe, e.g. answering whether or not diverse processes take place in their ejecta and the sources of different emission components, a large sample of sources are necessary (Andreoni et al. 2021, 2022). However, obtaining such a large data set is a difficult task for several reasons. Firstly, KNe are rare (< 1 per cent of the core collapse supernova rate), fast (rapidly fading $\gtrsim 0.5$ mag per day in the optical), and faint transients ($M \gtrsim -16$ at peak), e.g. see Andreoni et al. (2022). Secondly, the typical protocol for identifying and studying KNe remains, for the most part, rapid follow-up of gravitational-wave (GW) and high-energy gamma-ray burst (GRB) triggers (e.g. Andreoni et al. 2021, 2022). So far, the only GW detection that led to the discovery of a KN counterpart was the BNS merger GW170817, and even with near-term improvements to GW monitoring networks only a few tens of triggers are anticipated throughout the upcoming decade (see Andreoni et al. 2019).

Current and future wide-field optical and near-infrared surveys have been recently employed as tools for discovering KNe (Andreoni et al. 2019, 2021, 2022). The fundamental idea is to capitalize on real-time survey data for serendipitous transient discovery, as opposed to 'triggered' observations that use timing and/or localization information from other wavelengths or messengers (Andreoni et al. 2021). Active facilities applicable for serendipitous fast-transient discovery include the Panoramic Survey Telescope and Rapid Response System (Pan-STARRS; Morgan et al. 2012), Asteroid Terrestrial-impact Last Alert System (ATLAS; Tonry et al. 2018), the Dark Energy Camera (DECam; Flaugher et al. 2015), the Zwicky Transient Facility (ZTF; Bellm et al. 2019; Graham et al. 2019; Masci et al. 2019; Dekany et al. 2020; Ho et al. 2022), and the Gravitational-Wave Optical Transient Observer (GOTO; Gompertz et al. 2020), while future instrumentation include BlackGEM (Bloemen et al. 2015) and the Vera C. Rubin Observatory's Legacy Survey of Space and Time (LSST; Ivezić et al. 2019).

The ZTF has been a particular focal point for serendipitous KN discoveries as its volumetric survey speed is sensitive to objects that are faint and fast-fading out to almost 200 Mpc (Andreoni et al. 2021), and its alert stream design follows closely that envisioned for the LSST (Patterson et al. 2019). The ZTF was built upon the existing Palomar 48 arcsec telescope after being equipped with a custom-built wide-field camera (e.g. Bellm et al. 2019), and its observing system scans large areas of the sky several times each night in multiple bands ($g' r' i'$), with optical transients identified in near-real time using reference image subtraction (Dekany et al. 2020).

A first initiative (Andreoni et al. 2021) was developed as the ZTF REaltime Search and Triggering (ZTFReST) to identify KNe in ZTF data, and autonomously rank candidates in the ZTF alert stream based on their photometric evolution and fitting to KN models. Though ZTFReST proved to be effective at serendipitously discovering extragalactic fast transients in the initial system-test trials carried out by Andreoni et al. (2021), no KNe were identified. Such results, in addition to outcomes from simulation studies of Vera C. Rubin Observatory observations (e.g. Andreoni et al. 2022), have raised the necessity of exploring alternate strategies for synoptic survey techniques and alert characterizations that are optimized to study the transient universe (e.g. see Andreoni et al. 2019; Almualla et al. 2020).

In this article, we propose a method to explore the detection and early characterization of potential KN candidates from the public data released by ZTF in real time. We use FINK[1] (Möller et al. 2020), a

community broker for the upcoming LSST, which currently analyses the public alert stream from the ZTF survey. We have built three specific selection algorithms (known as 'filters') to select the most promising KN candidates from the global alert streams. The KN filters are based on temporal light curve and colour evolution, and will be explained in detail in Section 3.2.

We demonstrate the ability of the GRANDMA (Antier et al. 2020a, b) world-wide network of telescopes to respond quickly to ZTF-Fink alerts and provide complementary observations to ZTF data at very early times. From the actual cadence of ZTF, we expect a collection of consecutive points, taken with the same filter, to have ~2.5 d cadence. However, works such as Coughlin et al. (2020d), Almualla et al. (2021) demonstrate that there is added value in obtaining a more refined sampling resolution for the light curve of the transient due to the fast-fading nature of KNe. Early-time observations are especially important in bluer bands such a B or g', in which the KN is expected to fade even more quickly – becoming undetectable within on the order of one or two days. In addition, incorporating different filter combinations can help in distinguishing KNe from other candidate transients through their expected colour evolution (Margutti et al. 2018; Cowperthwaite et al. 2019; Coughlin et al. 2020d).

The main challenge is not only to coordinate responses to alerts within 48 h globally, but also to build a real-time data reduction pipeline that is able to digest heterogeneous data from a diverse set of telescopes in order to produce refined data in between consecutive ZTF observations. Although this general problem of calibration, explored for example in Perley et al. (2019), Brennan & Fraser (2022), is not new, it is crucial for the progress of transient and GW science. The larger objective is therefore to efficiently characterize all of the candidate transients through the use of optimal filter choices and multiple early-time observations, in order to rapidly rule out (or confirm) the nature of the transient as a KN.

We organized an observational campaign from 2021 May 21 to 2021 September 21, named 'ReadyforO4' (RO4), to invite members of GRANDMA (both professional and amateur astronomers) to follow-up KN candidates from ZTF-Fink in order to enable the early characterization of the detected transients. The paper is organized as follows: Section 2 introduces the GRANDMA consortium, and its citizen science program, Kilonova-catcher. Section 3 provides details on the KN filters used in this work, provided by FINK in collaboration with GRANDMA. Section 4 presents the GRANDMA observations of the RO4 campaign, general data reduction, accuracy of real-time scoring, and the results for non-confirmation of KNe. We finish by presenting our conclusions in Section 5.

2 GRANDMA AND KILONOVA CATCHER

The GRANDMA (Global Rapid Advanced Network Devoted to Multimessenger Addicts) consortium is a world-wide network of 30 telescopes from 23 observatories, 42 institutions, and groups from 18 countries (e.g. see Antier et al. 2020a, b). These facilities make available large amounts of observing time that can be allocated for photometric and/or spectroscopic follow-up of transients. The network has access to wide field-of-view telescopes ([FoV] >1 deg^2) located on three continents, and remote and robotic telescopes with narrower fields-of-view as reported in Table 1.

New telescopes have joined the network since the third LIGO-Virgo observational run O3 (which was described in Antier et al. 2020a, b). In particular, the collaboration with Thailand has provided an opportunity to access both the Southern and Northern sky by Thai Robotic Telescopes (TRTs) located at Springbrook Observatory

Table 1. List of telescopes of the GRANDMA consortium and their photometric performance when using their standard setup. In blue are mentioned the ones that were engaged in observations for this work.

Telescope Name	Location	Aperture (m)	FOV (deg)	Filters	3σ limit (AB mag)	Max. Night slot (UTC)
TRT-SBO	Sierra Remote Obs.	0.70	0.17×0.17	$UBVR_CI_C$	19.0 in 60s (Clear)	00h–10h
TAROT/TCH	La Silla Obs.	0.25	1.85×1.85	Clear, $g'r'i'$	18.0 in 60s (Clear)	00h–10h
TRT-SRO	Springbrook Research Obs.	0.70	0.17×0.17	$UBVR_CI_C$	19.0 in 60s (Clear)	10h–16h
CFHT/WIRCAM	CFH Obs.	3.6	0.35×0.35	JHK_S	22.0 in 200s (J)	10h–16h
FRAM-Auger	Pierre Auger Obs.	0.30	1.0×1.0	BVR_CI_C, Clear	17.0 in 120s (R_C)	00h–10h
CFHT/MEGACAM	CFH Obs.	3.6	1.0×1.0	$g'r'i'z'$	23.0 in 200s (r')	10h–16h
Thai National Tel.	Thai National Obs.	2.40	0.13×0.13	Clear, $u'g'r'i'z'$	22.3 in 3s (g')	11h–23h
Zadko	Gingin Obs.	1.00	0.17×0.12	Clear, $g'r'i'I_C$	20.5 in 40s (Clear)	12h–22h
TNT	Xinglong Obs.	0.80	0.19×0.19	$BVg'r'i'$	19.0 in 300s (R_C)	12h–22h
Xinglong-2.16	Xinglong Obs.	2.16	0.15×0.15	$BVRI$	21.0 in 100s (R_C)	12h–22h
GMG-2.4	Lijiang Obs.	2.4	0.17×0.17	$BVRI$	22.0 in 100s (R_C)	12h–22h
BJP/ALi-50	ALi Obs.	0.5	0.38×0.38	*Clear*, $g'r'$	20.8 in 20s (Clear)	14h–00h
UBAI/NT-60	Maidanak Obs.	0.60	0.21×0.21	BVR_CI_C	18.0 in 180s (R_C)	14h–00h
UBAI/ST-60	Maidanak Obs.	0.60	0.23×0.23	BVR_CI_C	18.0 in 180s (R_C)	14h–00h
TAROT/TRE	La Reunion	0.18	4.2×4.2	Clear	16.0 in 60s (Clear)	15h–01h
Les Makes/T60	La Reunion.	0.60	0.3×0.3	Clear	19.0 in 180s (Clear)	15h–01h
Terskol/Zeiss-600	Terskol Obs	0.6	0.18×0.18	Clear, BVR_CI_C	21.5 in 120s (R_C)	16h–02h
Abastumani/T70	Abastumani Obs.	0.70	0.5×0.5	BVR_CI_C	18.2 in 60s (R_C)	17h–03h
ShAO/T60	Shamakhy Obs.	0.60	0.28×0.28	BVR_CI_C	19.0 in 300s (R_C)	17h–03h
Lisnyky/AZT-8	Kyiv Obs.	0.70	0.38×0.38	$UBVR_CI_C$	20.0 in 300s(R_C)	17h–03h
Lisnyky/Schmidt	Kyiv Obs.	0.36	0.20×0.14	Clear, $UBVR_CI_C$	19.5 in 300s(R_C)	17h–03h
TAROT/TCA	Calern Obs.	0.25	1.85×1.85	Clear, $g'r'i'$	18.0 in 60s (Clear)	20h–06h
FRAM-CTA	ORM	0.25	0.43×0.43	Clear, BVR_Cz',	16.5 in 120s (R_C)	20h–06h
IRIS	OHP	0.50	0.4×0.4	Clear, $u'g'r'i'z'$	18.5 in 60s (r')	20h–06h
T120	OHP	1.20	0.3×0.3	BVR_CI_C	20.0 in 60s (R)	20h–06h
Pic du Midi/T1M	Pic du Midi	1.05	0.13×0.13	$u'g'r'i'z'$	19.5 in 60s (r')	20h–06h
2.2m CAHA/CAFOS	Calar Alto Obs.	2.20	$0.27\bigcirc$	$u'g'r'i'z'$	23.7 in 100s (r')	20h–06h
3.5m CAHA/Ω2000	Calar Alto Obs.	3.50	0.257×0.257	JHK_S	20 in 90s (J)	20h–06h
10.4m GTC/OSIRIS	ORM.	10.40	0.13×0.13	$u'g'r'i'z'$	24 in 30s (r')	20h–06h
10.4m GTC/EMIR	ORM.	10.40	0.111×0.111	$YJHK_S$	24 in 120s (Y)	20h–06h
VIRT	Etelman Obs.	0.50	0.27×0.27	$UBVR_CI_C$, Clear	19.0 in 120s (Clear)	22h–04h
Perkin-Elmer Tel.	Pico dos Dias Obs	1.6	0.083×0.083	$UBVR_CI_C$	21 in 360s(Clear)	18h–01h

(TRT-SBO) in Australia and Sierra Remote Observatory (TRT-SRO) in USA.

The 50 cm Ali telescope of the Beijing Planetarium, Beijing Academy of Science and Technology, performs both astronomy research and public outreach functions. It is located in the Ngari region of Tibet. It is a 20 arcsec reflecting telescope equipped with a 22.5mm × 22.5mm CMOS camera. The 5σ magnitude limits are expected to be $g' > 20$ mag in single images.

A 38 cm Schmidt-Cassegrain (with f/11 equipped with an ST-8 CCD sensor) was used at the Lisnyky Observatory granted by the Main Astronomical Observatory of National Academy of Sciences of Ukraine.

The ICAMER (International Centre for Astronomical, Medical and Ecological Research) Observatory of the National Academy of Science of Ukraine provided observations with the 60 cm Zeiss at the Terskol Observatory located in the North Caucasus.

In addition, the 1 m telescope in Pic du Midi is being renovated by the Institut de Recherche en Astrophysique et Planétologie (IRAP) and will participate in the GRANDMA consortium, as well as the 1.6 m Perkin-Elmer telescope located at Pico dos Dias Observatory in Brazil. All characteristics of the new partners can be found in Table 1.

Within 24 h, the GRANDMA network is able to access more than ∼72 per cent of the sky (up to more than 80 per cent) to a limiting

magnitude of ∼18 mag AB. Due to a less dense distribution of Western Hemisphere observatories, the sky coverage is reduced to 49–60 per cent during the night in the Americas. GRANDMA has access to four spectroscopic instruments with sensitivity down to ≈22 mag as shown in Table 2. In particular, the High-Energy Transients and their Hosts (HETH) group at the Instituto de Astrofísica de Andalucía has access to two telescopes via competitive proposals for orphan KNe. At the Centro Astronómico Hispano en Andalucía (CAHA), Almeria, Spain, we obtained observing time (PI: Kann) at the 2.2 m telescope (equipped with the Calar Alto Faint Object Spectrograph [CAFOS] and the Bonn University Simultaneous CAmera [BUSCA] optical imagers) and the 3.5 m telescope (with the Ω2000 infrared imager). Two nights of Ω2000 time were granted. At the 10.4 m Gran Telescopio Canarias (GTC), we obtained observing time (PI: Kann) with three instruments: the optical imager and spectrograph OSIRIS (Optical System for Imaging and low-Intermediate-Resolution Integrated Spectroscopy, 8 h), the infrared imager and spectrograph EMIR (Espectrògrafo Multiobjeto Infra-Rojo, 5 h), and finally the integral-field-unit spectrograph MEGARA (Multi-Espectrógrafo en GTC de Alta Resolución para Astronomía, 2 h) to obtain late-time 3D spectroscopy of KN host galaxies. As this is competitive time, we were more conservative with triggering; in particular the GTC proposal was focused on obtaining data from confirmed KNe only. Therefore no observations were obtained during this campaign. Fi-

Table 2. List of telescopes of the GRANDMA consortium with spectroscopic capabilities.

Telescope/Instrument	Location	Wavelength range	Spectral resolution $\lambda/\Delta\lambda$	Limiting mag
2.2m CAHA/CAFOS	Calar Alto Obs.	3200-7000/6300-11000	400	20 in 1h
ShAO/T2m	Shamakhy Obs.	3800–8000	2000	17 in 1h
Terskol-2m/MMCS	Terskol Obs.	3800–9000	1200	17 in 1h
Xinglong-2.16/BFOSC	Xinglong Obs.	3600–9600	1000	18 in 1h
GMG-2.4/YFOSC	Lijiang Obs.	3400–9100	2000	19 in 1h
10.4m GTC/OSIRIS	ORM	3630–7500	1018	22.5 in 1h
10.4m GTC/EMIR	ORM	890–13 310	987	20.5 in 1h
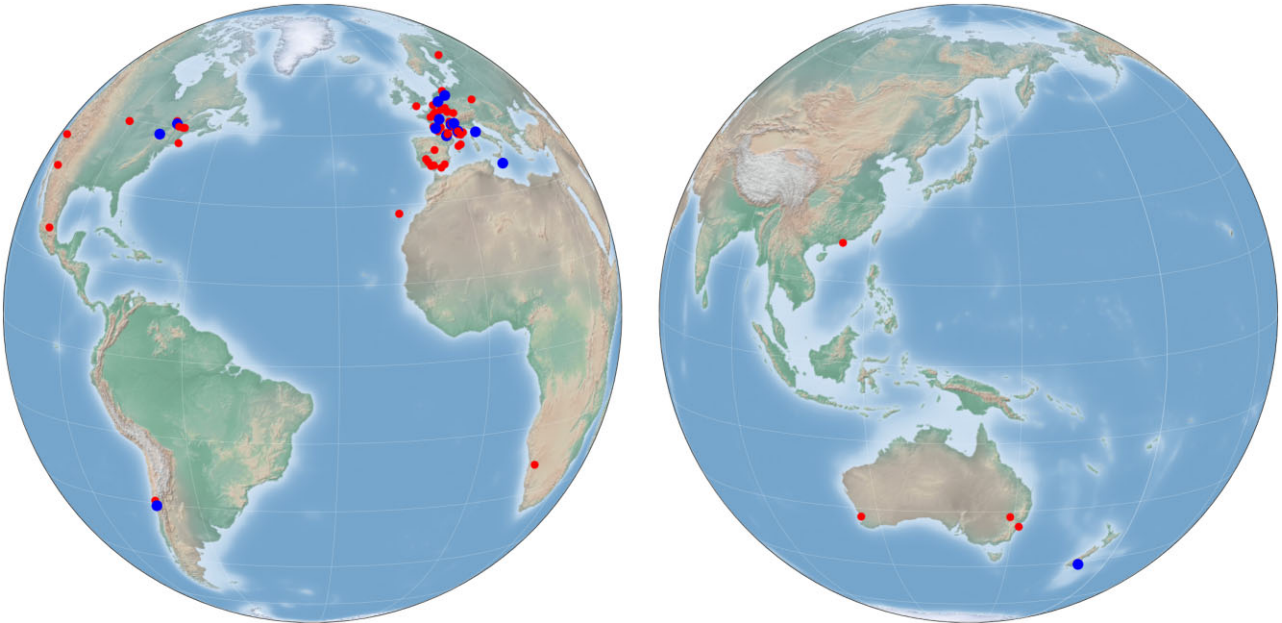
Figure 1. Locations of the 77 telescopes involved in the GRANDMA citizen science program *Kilonova-Catcher*. In blue are the telescopes used in this study, in red, the rest of the network.

nally, GRANDMA obtained 6 h time allocated by WIRCAM (Wide-field InfraRed Camera mounted on the Canada–France–Hawaii Telescope) in 2021A and 2021B that were not used due to the lack of confirmed KNe.

In 2019, GRANDMA initiated the creation of an innovative citizen science program called *Kilonova-Catcher*, hereafter KNC (Antier et al. 2020a). It aims at incorporating amateur astronomers into the search for and follow-up of fast transients such as GRBs and KNe. The GRANDMA consortium has already demonstrated its ability to forward the alerts of the O3 observing run to the amateur astronomers and to provide customized observation plans to each KNC astronomer; in return, they transfer images to the GRANDMA server to be analysed afterwards. This process creates a continuous chain of observations at very early times after the alerts, before passing the responsibilities to the larger aperture telescopes of the professional community. KNC uses a dedicated portal[2] to organize its activities, while the GRANDMA consortium is in charge of the data analysis of the images (see Section 4). In Fig. 1, we show the locations of the KNC telescope network.

[2]http://kilonovacatcher.in2p3.fr/ supported by the University of Paris and the IJCLab institute

3 METHOD: SEARCHING FOR KILONOVAE USING THE FINK BROKER

3.1 FINK overview

FINK (Möller et al. 2020) is a community broker designed to enable science with large time-domain alert streams such as the one from the current ZTF survey or the upcoming LSST. Driven by its scientific community, FINK probes a large number of topics in the transient sky, from Solar system science to galactic, and extragalactic science.

FINK currently analyses the public alert data stream from the ZTF survey. Each night, alerts are collected in real-time after their processing by ZTF. FINK received 35 387 098 alerts between 2021 April 1 and September 30 (160 observing nights). Alerts carry out basic measurements for the trigger (position, magnitude, time), but also the detections that occurred up to 30 d before the alerts at the same location in the sky, allowing us to reconstruct at least a partial light curve of the potential candidate. All incoming alerts are stored on disc, but only alerts with sufficient quality are then processed. At the time of the campaign, there were three quality cuts in FINK to assess the quality of alerts and reject artefacts and known bogus alerts (Möller et al. 2020): (1) the RealBogus score assigned by the ZTF alert distribution pipeline (Duev et al. 2019) must have a value above 0.55, (2) there should be no prior-tagged bad pixels in a 5×5 pixel stamp around the transient, and (3) the difference
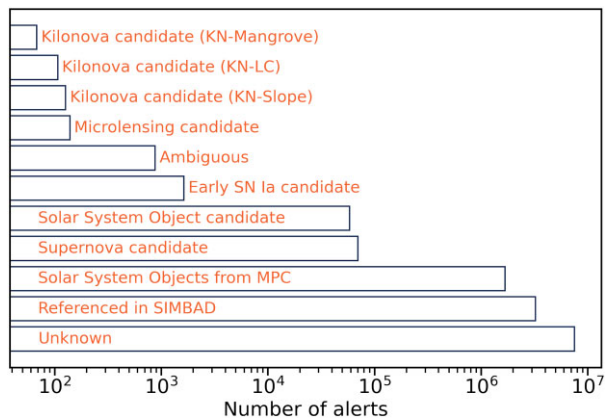
Figure 2. FINK classification labels for the 12 556 539 ZTF alerts that passed the quality cuts in the period 2021 April 1 to September 30. About half of the alerts got no classification (Unknown label), i.e. FINK was not able to conclude on the nature of the alert given the alert information available. The remaining half is dominated by objects with a counterpart in the SIMBAD data base (match within 1″.5 radius), and alerts associated with a known object from the Minor Planet Center data base (moving objects from the Solar System). Other alerts are associated with supernova events, Solar System Object candidates, microlensing candidate events, or have an ambiguous classification (more than one label at a time). Concerning KN candidates, we report here the candidates from the three filters (see the text below).

between the aperture magnitude and the PSF-fit magnitude must be lower than 0.1 mag (in absolute value). These cuts discarded about 70 per cent of the incoming alerts.

The remaining 30 per cent of alerts (12 556 539 alerts) are then processed by the FINK science modules. Science modules are provided by the community of users to add value to alerts, as detailed below. We note that the state of the broker constantly evolves over time (additions, or corrections), and we report results using `fink-broker` version 1.1, `fink-science` version 0.4, and `fink-filters` version 0.2. There are several types of added values: labels from the cross-match with external catalogues or survey feeds, classification scores provided by a machine learning analysis, or simply tags based on the alert content. These added values are then combined to provide a unique classification for each alert. Fig. 2 shows the alert classification during the KNC observational campaign.[3] About half of the alerts got classified, i.e. FINK can extract information about the potential nature of the object. Most of the classified alerts are catalogued in the SIMBAD data base or correspond to objects identified in the Minor Planet Center.[4]

3.2 Kilonova candidate selection

Our main goal is to identify the most probable KN candidates among all incoming alerts. There are two competing factors: criteria that are too broad would yield too many candidates to follow up, given the huge number of incoming alerts; on the other hand, complex selection criteria would be meaningless given the lack of actual KN observations to constrain the parameter space.

---

[3]The definition of the classification is made by the members of FINK and it evolves over time as our knowledge improves. See https://github.com/astrolabsoftware/fink-filters/blob/master/fink_filters/classification.py for more information.

[4]https://www.minorplanetcenter.net/

In order to optimize our search for KNe, we designed three selection filters targeting different likely aspects of a KN. They act at the end of the FINK processing to reduce the incoming data stream and to select the most probable KN candidates. In the period of 2021 April 1 to September 30 we obtained:

(i) Machine learning-based filter (KN-LC): 107 alert candidates
(ii) Near-by Galaxy Catalogues-based filter (KN-Mangrove): 68 alert candidates
(iii) Rate-based filter (KN-Slope): 127 alert candidates

We note that only five alert candidates were selected by more than one filter, showing that the filters are triggered by different parameters of the incoming alerts. Hence, alerts selected by more than one filter are particularly noteworthy. All filters are open-source and can be found at https://github.com/astrolabsoftware/fink-filters. A detailed description and analysis of the filter outputs can be found in the accompanying notebook.[5]

3.2.1 Machine learning-based filter (KN-LC)

This filter mainly uses information from the light curve. During the classification step, the FINK classifier extracts features from the light curves in the g' and r' photometric bands (see Biswas et al., in preparation) and infer the probability of an alert being a KN. The light curves are deconstructed as a linear combination of principal components, and additional features are also extracted such as the maximum of the flux, residuals, and the number of measurements. Because we have better accuracy with more principal components, choosing the number of principal components is a compromise between the efficacy of the classifier and the amount of time that is needed to classify alerts and identify candidates (the more components, the more measurements we need, see Biswas et al., in preparation for more details).

In the early days of the campaign, we were using only the first principal component. However, it was shown quickly that one component was not sufficient to produce a reliable score on the alert data, and we had many false-positives (e.g. many candidates were obvious supernovae). So we introduced the second principal component in the set of features for the classification, and the results with real data improved without introducing further delays in practice given the cadence of the ZTF survey (that is without the need to add more measurements). In addition, the average number of candidates per month was reduced, from about 28 candidates per month to about 10 per month. The change of the model in the classifier happened on 2021 June 17. In FINK, data and model are versioned, and the new model corresponds to the version 0.4.5.

This filter uses the five following criteria:

(i) The score from the KN classifier must be above 0.5 (binary random forest classifier).
(ii) Point-like object: the star/galaxy extractor score provided by ZTF must be above 0.4 (Tachibana & Miller 2018).
(iii) Non-artefact: the deep real/bogus score provided by ZTF (Duev et al. 2019) must be above 0.5.
(iv) Object not referenced in the SIMBAD data base (except from extragalactic origin).
(v) Young detection: less than 20 d. This threshold is quite loose but it is sufficient to filter long-trend or well-known objects.

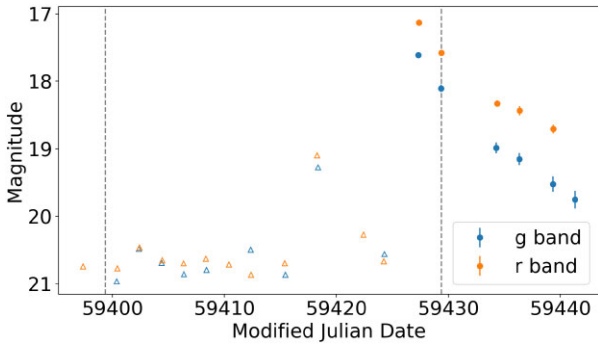[5]https://github.com/astrolabsoftware/fink_grandma_kn

Figure 3. ZTF object light curve of one kilonova candidate from the KN-LC filter. Circles with error bars show valid alerts (detections) that pass the FINK quality cuts. Downward-pointing open triangles represent 5σ magnitude limits in template-subtracted difference images based on point-spread-function (PSF) fit photometry contained in the history of valid alerts. The right-most vertical line shows the KN trigger by FINK, and data used to classify the alerts are shown in between dashed vertical lines (30-d history data are attached with the alert). The alert leading to the KN trigger, ZTF21abqfzcp, was emitted on 2021 August 3 08:51:48 UTC. On the next re-observing night (five days after), new photometric data from alerts favoured a supernova candidate classification, ruling out the nature of the transient being a KN.

Over the campaign, this filter selected 107 alert candidates out of 12 556 539. This corresponds to 70 unique objects on the sky (the same astrophysical objects can emit several alerts over time). Fig. 3 shows the light curve of such a candidate. All objects are labelled in the FINK data base and can be easily accessed via the Science Portal.[6]

With time, FINK collects more alert data, and has a clearer view on the nature of each object. At the end of the campaign, we found that most objects that emitted at least one alert tagged as KN candidates were deemed to be supernova candidates; however, some remained as KN candidates.

We also performed a cross-match with the data from the Transient Name Server. Considering only the candidates from the first model (before 2021 June), most of the candidates turned out to be Type Ia supernovae (41/71). However, after the model used to classify alerts changed, 29/36 of the candidates had no counterpart in the Transient Name Server (i.e. there was no follow-up), the others being identified as cataclysmic variables (6/36) or Type IIb supernovae (1/36).

3.2.2 Near-by galaxy catalogues (KN-Mangrove)

With the previous filter, KN-LC, we concluded that a minimum of two days from the first detection by ZTF is necessary to get a reliable score from the classifier and to identify candidates. According to KN models, two days after the compact binary merger, the signal will be fading or even too faint to be observed. So we developed a second filter to address younger detections. This filter uses the following criteria:

(i) Point-like object: the star/galaxy extractor score must be above 0.4.

(ii) Non-artefact: the deep real/bogus score must be above 0.5.

(iii) Object not referenced in the SIMBAD data base (except from extragalactic origin).

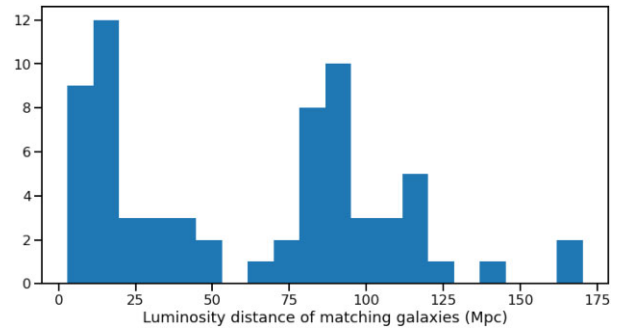(iv) Young detection: less than 6 h.

Figure 4. Histogram of the luminosity distance of galaxies associated with alerts selected by the KN-Mangrove filter. For the campaign, we only considered the galaxies from the Mangrove catalogue in a 230 Mpc range, corresponding to the observation range of current GW detectors. In practice, we have no candidates further than 170 Mpc. Alerts and galaxies are matched within a radius of 10 kpc. The threshold has been set such as to avoid a large number of spurious associations in the observation plane, while allowing coverage around the galaxy. Note that the allowed angular distance between alerts and galaxies increases when the luminosity distance decreases, hence leading to more frequent spurious associations at small luminosity distances.

(v) Galaxy association: the alert should be within 10 kpc of a galaxy from the Mangrove catalogue. The 10 kpc is empirical (see discussion in Berger 2014) – we also tested different values. Above 10 kpc, we have a very large rate of contaminants. Below 10 kpc, we would potentially miss valid transients.

(vi) Absolute magnitude: the absolute magnitude of the alert should be -16 ± 1 mag (in both g' and r' bands).

(vii) Non-Solar System Object: the alert must be at least 5 arcsec away from any known Solar System objects referenced in the Minor Planet Center data base at the time of emission.

With the KN-Mangrove filter, an alert will be considered as a candidate if one can identify a suitable host and the resulting absolute magnitude is compatible with KN models. To identify possible hosts, we used the MANGROVE catalogue (Ducoin et al. 2020), containing about 800 000 nearby galaxies. For the campaign, we only considered galaxies within 230 Mpc, as it corresponds to the current observation range of GW detectors. Fig. 4 shows the distribution of luminosity distances of galaxies associated with alerts selected by the KN-Mangrove filter.

In practice, the galaxy association method is not perfect, and can lead to misassociation of an event that is in the foreground or the background of a galaxy.[7] But this is inevitable, as the luminosity distance between the Earth and the source generating the alert is usually unknown.

According to Kasliwal et al. (2020), we expect a KN event to have a peak absolute magnitude at $g' \sim -16$ mag. This threshold is given in g'-band, but in this work it was implemented for g' and R' bands without distinction. This hypothesis is due to the lack of early observations and strong consistency with AT2017gfo (Abbott et al. 2017b). As we often do not know the source distance, we compute the absolute magnitude from an alert as if it were in the matched galaxy.

[7]See for example https://fink-portal.org/ZTF21abdwdwo that was selected by the KN-Mangrove filter and associated with the bright LEDA 1740743 galaxy in Mangrove. After visual inspection, it turns out that the alert more likely originated from a fainter galaxy located further away, and not present in Mangrove.

68 alert candidates were selected by this filter out of 12 556 539 processed alerts from 2021 April 1 to 30 September 30. This corresponds to 59 unique objects on the sky. At the end of the campaign we checked, using more data, the evolution of the classification of those objects. We found that most objects remained KN candidates according to the KN-Mangrove classifier, while a small fraction were subsequently identified as potential supernova candidates or Solar System Object candidates. This was confirmed when checking against Transient Name Server data, where we found 51/68 alerts without a counterpart (i.e. no follow-up result was reported), 7/68 confirmed as supernova type Ia, 4/68 as supernova type II, 3/68 as supernova type IIp, 1/68 as supernova type IIb, 1/68 as supernova type Ib, and 1/68 as supernova type Ic.

3.2.3 Slope-based filter (KN-Slope)

In addition to the two previous filters, we developed a third filter based on the work of Andreoni et al. (2021). The main criterion used for extracting KN candidates corresponds to the slope of the normalized light curve (mag d^{-1}). Given the expected light curves of KNe, we chose a threshold of 0.3 mag d^{-1}, which corresponds to a fast-fading object. This filter was not adopted during the campaign as it did not provide satisfying results. However for reference we reprocessed the campaign data and we present its performance here. This filter will be used in the subsequent campaigns along with the two other filters. In total, this filter implements eight criteria:

(i) Fast fade: The apparent magnitude decay rate of the alert must be above 0.3 mag d^{-1} in the last photometric band with two sequential measurements.

(ii) Point-like object: The star/galaxy extractor score of the alert must be above 0.4.

(iii) Non-artefact: The deep real/bogus score of the alert must be above 0.9.

(iv) Object not referenced in the SIMBAD data base (except from extragalactic origin).

(v) Object not referenced in the Sloan Digital Sky Survey (SDSS) as a star or quasi-stellar object.

(vi) Young detection: The alert emission date must be less than 14 d. In practice the delay between the first detection and the trigger by FINK is a maximum two days (two consecutive measurements by ZTF).

(vii) Non-Solar System Object: The alert must be at least 10 arcsec away from any known Solar System objects referenced in the Minor Planet Center data base at the time of emission.

(viii) Away from the galactic plane: The alert must have an absolute galactic latitude above 10 deg.

127 alert candidates were selected by this filter out of 12 556 539 processed alerts from 2021 April 1 to September 30. This corresponds to 108 unique objects on the sky. At the end of the campaign, most of the objects had produced more alerts after the initial KN trigger, and were mostly falling under the class of supernova candidates according to the FINK filters. When cross-matching with data on the Transient Name Server, 117/127 have no counterparts, 6/127 are from cataclysmic variables, 3/127 are from supernovae type Ia, and 1/127 is from supernova type IIn.

3.3 Accuracy, efficiency, and added value

The main purpose of the classifier is to identify the most probable fast transient candidates in the sample, with a particular focus on
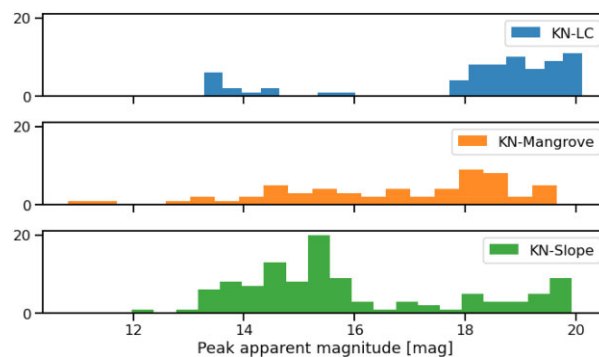

Figure 5. Histogram of the peak apparent magnitude for the candidates that pass the three filters: KN-LC (top, blue, see 3.2.1), KN-Mangrove (middle, orange, see 3.2.2), KN-Slope (bottom, green, see 3.2.3). In the case of the KN-LC and KN-Slope filters, the distributions have an excess of candidates at the two ends (faintest and brightest objects), while the peak apparent magnitude distribution in the case of KN-Mangrove is rather uniform across the magnitude range. The faintest peak apparent magnitude is around 20 mag for all filters.

KNe. However, to determine the nature of transients of interest, it generally requires follow-up photometry above and beyond what is provided by a survey with return time-scales of ∼1 night or more. For this reason, measurements of the number of transients passing the selection filters are required to understand the nature of objects that will pass those filters. In particular, empirical measurements of the rate of transients passing particular filters are useful for assessing the contamination rate and therefore the follow-up photometry (and potentially spectroscopy) required to characterize the sample.

To evaluate the contaminant rate, we re-analysed the ZTF alert stream data taken between 2019 November and 2021 September (538 observing nights), corresponding to 38 372 852 (12 149 579) processed alerts (unique objects). Using this data, 197 (132) alert candidates have passed the KN-LC filter, 227 (208) candidates passed the KN-Mangrove filter, and 285 (247) candidates passed the decay rate filter (KN-Slope). According to Transient Name Server classification data, for the KN-LC and KN-Mangrove filters, the most common contaminant transients were supernovae near peak,[8] and for the decay rate filter, the most common transients were fading cataclysmic variables near the Galactic plane. Given the ZTF coverage, this corresponds to a magnitude-limited rate of about 0.5 candidates per night per filter down to a magnitude of 20.5. Fig. 5 shows the histogram of the peak apparent magnitude for the candidates that pass the filters. While the KN-LC and KN-Slope distributions seem bi-modal (due to, for example, the excess of cataclysmic variables in the KN-Slope filter), the results from the KN-Mangrove filter are more spread across the magnitude range. Our analysis provides important information to understand the underlying population of contaminants (assuming there are no KNe) and also for future surveys as Vera Rubin LSST.

4 GRANDMA/KILONOVA-CATCHER RO4

We organized the 'ready for O4 campaign-I' to (i) demonstrate the potential of amateur astronomy in the search of GW counterparts, (ii) introduce the GRANDMA consortium into the search for KNe, and (iii) establish the caveats for performing joint photometry with

---

[8]Note that in the case of KN-Mangrove, we would have four times more candidates if we did not reject Solar System objects.
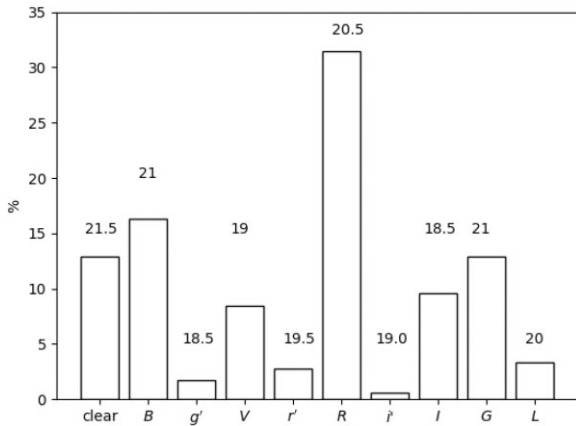
Figure 6. Filters used in the images taken during this observational campaign and when a source is detected. Above are mentioned the fainter upper limits reached during the campaign (see section 4.1).

different apertures and filters. From 2021 May 21 to 2021 September 21, we followed six alerts sent by our KN broker implemented in FINK (see Section 3) focusing on alerts sent on Friday. The aim was to invite amateurs to observe the transient during the next 72 h (so that the amateurs would have the weekend for performing observations), to verify how many would respond and with which latency. If no alert passed our thresholds, we provided the observers recent supernovae (three in our campaign) to be observed for practice purposes. In 2021 July, we invited all GRANDMA teams to observe kilonova candidates as well in order to have a larger set of images to test our photometric pipeline on heterogeneous data. Several online tutorials were organized allowing us to enroll a large number of amateurs with their respective observatories. A preliminary requirement file was released to indicate to the observers how to provide useful data for the campaign. In particular, we were first targeting a 'classification mode' requiring the use of several photometric bands to either confirm the event detection or reject it as a false alarm, and secondly a 'monitoring mode' by following up the multiband flux evolution of the transient source.

In total, we achieved participation by 26 amateurs and 11 distinct GRANDMA telescopes (see Table 2). We received images taken with filters in professional and amateur filter systems, and also images taken without filters (see Fig. 6).

4.1 Data reduction

In order to uniformly process the diverse set of images acquired by various telescopes, we developed two dedicated photometric pipelines: STDPIPE[9] (will be referenced henceforth as 'STD') and MUPHOTEN[10] (Duverne et al. 2022) (will be referenced as 'MU').

STDPipe – STDPIPE (Karpov 2021) is a set of Python routines for astrometry, photometry, and transient detection related tasks, intended for quick and easy implementation of custom pipelines, as well as for interactive data analysis. It is designed to operate on standard Python objects: NUMPY arrays for images, ASTROPY Tables for catalogues and object lists, etc., and conveniently wraps external codes that do not have their own Python interfaces (SExtractor (Bertin & Arnouts 1996), SCAMP (Bertin 2006), PSFEx (Bertin 2011a), HOTPANTS (Becker 2015), Astrometry.Net (Lang et al.

[9]STDPIPE is available at https://gitlab.in2p3.fr/icare/stdpipe
[10]MUPHOTEN is available at https://gitlab.in2p3.fr/icare/MUPHOTEN

2010), etc). It supports the following steps of processing and analysing the images:

(i) object detection and photometry using either SExtractor (Bertin & Arnouts 1996) or SEP (Barbary 2016) codes. Simple PSF photometry may be performed by the SExtractor backend using a PSF model estimated by the PSFEX (Bertin 2011b) software, or aperture photometry based on photutils (Bradley et al. 2021) may be run using various kinds of background estimation, either global or local.

(ii) astrometric calibration using Astrometry.net (Lang et al. 2010) for blind World Coordinate System (WCS) solving in either remote or locally installed variants, and using SCAMP (Bertin 2006) or custom Astropy-based code for astrometric refinement by matching the lists of objects detected in image with catalogue entries

(iii) photometric calibration using any catalogue available in Vizier as a reference with approximate on-the-fly passband conversion for some of them (in order to derive the magnitudes in the Johnson-Cousins system based on the ones in Pan-STARRS or *Gaia* systems). A sophisticated photometric matching routine is available for fitting the zero-point and photometric system of the frame taking into account a spatial polynomial of arbitrary order, a colour term, as well as an optional additive flux term.

(iv) image subtraction with the HOTPANTS (Becker 2015) code using either locally available templates or images automatically downloaded from the network. The code allows downloading templates either from the Pan-STARRS archive of stacked images (Waters et al. 2020), or from any imaging survey accessible through the HiPS2FITS (Boch et al. 2020) service. When running the image subtraction code, a custom noise model may be supplied in order to account for the poorly known gain and bias levels of the image.

(v) transient detection and photometry on difference images taking into account the proper noise model of the difference image and various artefact masks in order to decrease the number of false detections. The transients may be filtered based on coincidences with either locally available or remote catalogues, as well as with positions of known Solar System objects. Also, optionally a routine for sub-pixel adjustment of the transient cutout and template images may be performed in order to detect cases of slight positional shifts (causing 'dipoles' in difference images) either due to overall image misalignment, or object proper motion due to a large difference in the template epoch.

(vi) insertion of simulated stars with realistic PSFs into the images in order to assess the performance of transient detection.

(vii) the code also includes various convenience utilities and plotting routines for quick visualization of the results of every step.

The actual image processing pipeline for this work was organized as follows. As STDPIPE is intended for higher level analysis of pre-processed frames, we required all images to be pre-processed by an instrument-specific code to perform bias, dark subtraction, and flat-fielding in advance. Then we removed the cosmic rays using the astroscrappy (McCully & Tewes 2019) code implementing the original LACosmic (Dokkum (van) 2001) algorithm, and detected the objects on the image using SExtractor (Bertin & Arnouts 1996). Next, we performed aperture photometry with local background subtraction using a photometric aperture with radius equal to the median image full-width at half-maximum (FWHM), and a background annulus between radii of 5 and 7 FWHM units. Then, the astrometric solution was derived using the Astrometry.net (Lang et al. 2010) solver applied to the list of detected objects. Then, we downloaded the list of stars from the Pan-STARRS DR1 catalogue from Vizier to serve as both an astrometric and photometric reference catalogue, and augmented it with Johnson-Cousins B, V, R_C, and I_C magnitudes

using approximate conversions derived by Kostov & Bonev (2018). We refined the image astrometric solution using the SCAMP (Bertin 2006) code, via lists of detected objects and catalogue stars. Then we constructed the photometric solution for the image using the closest Johnson–Cousins filter as a reference and $B - V$ (or corresponding Pan-STARRS filter and $g_{ps1} - r_{ps1}$ for the telescopes using Sloan-like filter sets) as a colour used for deriving an instrumental photometric system (colour term). For the zero-point, we used either a constant value for all stars if the field of view (FOV) and number of stars were small, or a second-order spatial polynomial if there were enough stars in the frame. Then we downloaded the Pan-STARRS co-added images covering the observed field of view in the closest filters (either g_{ps1}, r_{ps1} or i_{ps1}), mosaicked them and used the result as a template which was then subtracted from the image using the HOTPANTS (Becker 2015) code. On the resulting difference image, we performed forced aperture photometry at the transient position using the same settings as used for deriving the original photometry, so that the zero-point model was still valid, and thus derived the transient photometry in a system linked to a standard one (either Johnson-Cousins or Pan-STARRS) by a colour term value specific for this frame. In a similar manner, we determined an effective detection limit at the transient position by converting the background noise inside the aperture multiplied by 5 (so that it corresponds to 5σ) to flux and then to the magnitude. When the object is not detectable in the image, this value was adopted as an upper (detection) limit for its magnitude.

In order to convert the results of this analysis to a standard photometric system one needs to know the colour of the transient at the moment of observations. It may be done either by combining several simultaneous or quasi-simultaneous observations in different filters (and thus with different colour terms) and then regressing for the colour from them, or using some external information. For the sake of the current analysis of transients detected by ZTF, we decided to use the colour estimate acquired from consecutive ZTF *g* and *r* band measurements, smoothly interpolated to the moment of observations and then converted to either $B - V$ or $g_{ps1} - r_{ps1}$, depending on the photometric system used for the calibration of the frame.

Muphoten – MUPHOTEN (Duverne et al. 2022) is a Python-based software dedicated to photometry of transients followed up by heterogeneous telescopes. It uses public Python libraries such as Photutils (Bradley et al. 2021), Astroquery (Ginsburg et al. 2019), and also uses external C codes: SExtractor (Bertin & Arnouts 1996), Scamp (Bertin 2006), Swarp (Bertin et al. 2002), and HOTPANTS (Becker 2015). The pipeline works on pre-processed images (dark or bias subtracted, flat-fielded) and for which an astrometric solution is known. For this campaign the astrometric calibration was done directly on the Astrometry.net website (Lang et al. 2010). The analysis process works as follows:

(i) subtraction of a Pan-STARRS template constructed with a mosaic of the observed FOV downloaded from the catalogue archives. For non-Sloan filters (e.g. Johnson-Cousins or unfiltered images), the closest band of the Pan-STARRS system was used: g_{ps1} for *B*, *V* and clear images, r_{ps1} for R_C images, and i_{ps1} for I_C.

(ii) background estimation in a mesh of 150×150 pixels, using the same estimator as SExtractor. The background is then subtracted from the image.

(iii) source detection using a 2σ threshold above the background.

(iv) aperture photometry on the detected sources.

(v) cross-match with Pan-STARRS catalogue to fit the instrumental magnitude versus Pan-STARRS magnitude relation with a linear fit. For images acquired using filters of the Johnson–Cousins photometric system, we used the second-order equations 1, 2, 4, and 6 of table 2 from Kostov & Bonev (2018) to transform the Pan-STARRS system to the observed filter. For clear images, we added the flux from the g_{ps1} and r_{ps1} Pan-STARRS bands.

(vi) detection of the transient in the residual image between the observed and the template images, adopting a 3σ threshold. A positive detection of a transient was considered if a source was identified at less than five pixels from the transient position.

(vii) evaluation of the transient instrumental magnitude in the residual image between the observed and the template image from the Pan-STARRS survey and usage of the previous fit to obtain the calibrated measurement of the transient.

MUPHOTEN uses two methods to filter out poor-quality images. One by comparing the calibrated magnitude of a star in the field of view to its magnitude in the catalogue used for the photometric calibration. If they are incompatible, the image is rejected. The second veto consists in computing the seeing of the image with PSFex (Bertin 2011a). Then for a given band of a given telescope + filter configuration, reject the images for which the seeing deviates by more than 3σ from the median seeing of the data set. For the images passing the vetoes with no detected transient, we set an upper limit on the magnitude. It is estimated by dividing the number of detected objects in the image by the number of objects in the reference catalogue in magnitude bins. When the result drops below 0.5, the centre of the corresponding bin is considered to be the limiting magnitude.

4.2 Consistency of the analysis

We processed the images using both the STDPIPE and MUPHOTEN pipelines, thus acquiring two independent sets of measurements based on different photometric models – one with a colour term for the former, and without it for the latter. While the former is more accurate in theory, it requires knowledge of a true transient colour at the time of measurement in order to convert the result to a standard photometric system. As described above, we rely on the colour information extracted from ZTF light curves (which is not necessarily complete and dense enough in time) to do it. On the other hand, MUPHOTEN calibration basically assumes that the colour of the transient is the same as the average colour of calibration stars used in the analysis.

Thus, the principal difference between the two pipelines we used is in how the colour of the object is handled, which may introduce a systematic colour-dependent bias to the photometric results. In order to assess this error, as well as other possible sources of bias, we compare the results of the two different methods in Fig. 7 for all the images where the transient is detected. The magnitudes estimated by STDPIPE and MUPHOTEN are typically well consistent within the error bars (see upper panel of Fig. 7), with the most significant differences being due to the images acquired in *B* filter or in white light (see lower panel of Fig. 7), i.e. when the impact of atmospheric conditions or the instrumental photometric system is expected to be maximal. Thus, we may conclude that there is no significant bias between the pipelines we used.

4.3 Rapid linear fit and offline classification

In this section, we will describe the linear fit and modelling to constrain the nature of the optical transients. Here, we call 'detection'
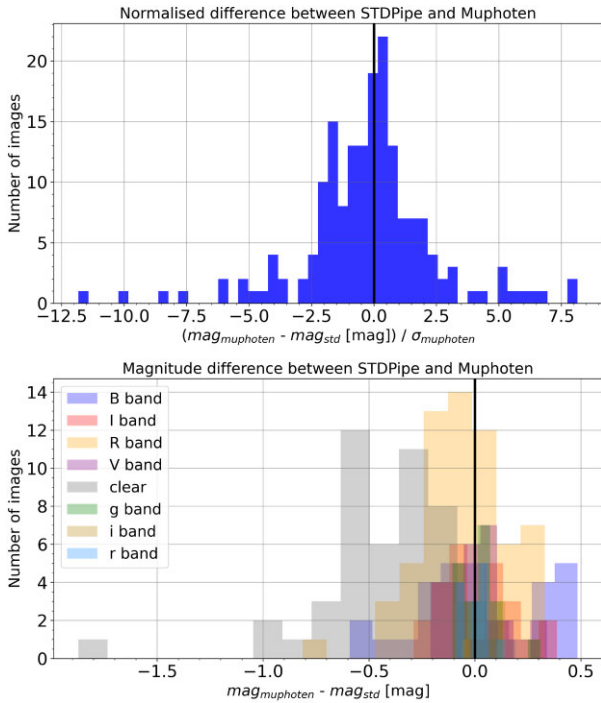
Figure 7. Comparison of the transient magnitudes estimated by two different pipelines. Upper panel – distribution of normalized differences, which is mostly consistent with the estimated error bars of individual measurements. Lower panel – absolute differences for individual photometric filters used.

the first public photometric detection of ZTF (defined as T_0). Images are grouped with 0.1 d precision. A group contains at least one image.

Linear fit method – Our goal was to identify transients undergoing rapid decrease or increase in brightness. We applied a linear regression procedure using a maximum-likelihood estimation approach to estimate the slopes between two different time bins, $t_i = T_0 + n_i$ d, where $n_i = 0.1 \times i$, and i is the index of a given time bin (see Appendix A). The slopes of the best fit, $a_r(t = n)$, are then computed using data taken with r or R filters in a given time bin. We actually computed three slopes:

(i) $a_{\mathrm{STD},r}(t = n)$, the temporal slope of the transient light curve between the first detection by ZTF at T_0 and the time at which GRANDMA detected it by using STDPIPE.

(ii) $a_{\mathrm{MU},r}(t = n)$, the temporal slope of the transient light curve between the first detection by ZTF at T_0 and the time at which GRANDMA detected it by using MUPHOTEN.

(iii) $a_{\mathrm{ZTF},r}(t = n)$, the temporal slope of the transient light curve between the first detection by ZTF at T_0 and the next detections by ZTF.

Offline source modelling - We constrained the nature of rapidly evolving optical transients using four light curve models a posteriori. For each of these models, we evaluate its degree of correlation with the observational data. We will use a KN model taken from Kasen et al. (2017) (Ka2017), a GRB afterglow (TrPi2018, Troja et al. 2018), the nugent-hyper model which creates supernovae light curve (nugent-hyper; Levan et al. 2005) and a shock cooling supernova light-curve model (Piro2021; Piro, Haynie & Yao 2021). The ideal model is one that has a regression consistent with the light-curve points as assessed by the Bayes factor of the model.

4.4 Results

In the following section, we summarize our observations and analyse the results produced by both STDPIPE and MUPHOTEN to extract information about the nature of the transients (see Fig. 8). We use MUPHOTEN for evaluating the upper limit of the image when no source has been detected by both pipelines independently. If the two pipelines provided inconsistent results for an image that had not been previously rejected, we excluded it from further analysis. Some GRANDMA teams performed their own measurements, but in order to keep a consistent analysis, they are not presented in this article. All our results are presented in table B2.

4.4.1 KN-Mangrove alert candidates

ZTF21abdwdwo was observed by eleven amateur telescopes with a total of 42 images taken from 0.7 to 9 d after the public detection (2021 June 4 04:27:26 UTC) (see Table B1). The associated alert was sent by FINK without any further delay. All images resulted in non-detections with a median upper limit of 17.9 ± 0.8 mag in the r' and R-band filters. An unfiltered image taken by the T40-A77DAU telescope 0.8 d post-detection yielded a 20.7 mag limit. T-CAT obtained the deepest upper limit ($\sim$21 mag in B- and G-band) 3.7 d post-detection (2021 June 7 21:41:04). At a much later date, the VIRT telescope confirmed the previous non-detections on 2021 August 3, 60 d post-detection with an upper detection limit of $R = 17.5$ mag. Our refined analysis showed there was a misassociation of the new source and the possible galaxy (see Section 3.2.2). In summary, GRANDMA follow-up classified the new source as a Solar System Object 0.8 d after ZTF discovery.

ZTF21abfmbix (later renamed SN 2021pkz, associated with the galaxy 2MASS-12551554+0253477 at 38 Mpc) was observed by 13 different amateur telescopes and FRAM-Auger with a total of 29 images taken between 0.7 and 50.8 d after T_0 (2021 June 11 05:14:49). The associated alert was sent by FINK with a 1.5 h delay. Two days before, ZTF did not detect any source brighter than $g' > 20.5$. A positive detection was found in 24 of the 29 images, using both the STDPIPE and MUPHOTEN pipelines. These images were taken in six different filters and also with no filter from 0.7 to 29.7 d post-detection. The next public ZTF measurement ($g' = 17.1$ mag, $r' = 16.9$ mag) was delivered two days after the first detection. We note that 17 of 25 photometric measurements (68 per cent) delivered from STDPIPE and MUPHOTEN are consistent within 0.1σ. We also note a maximum deviation of 0.6 mag in the L band and for images taken with no filter, when comparing the results of both pipelines. According to the results obtained with both pipelines, the data clearly show a transient in rising phase in the r' band. We evaluated the slopes of the luminosity rate (see Section 4.3) as: $a_{\mathrm{STD},r}(t = 0.7) = -0.7 \pm 0.2$ mag d^{-1} and $a_{\mathrm{MU},r}(t = 0.7) = -0.9 \pm 0.2$ mag/day. It is clear that the source is brightening. We also found agreement between the slope of the luminosity rate using the different pipelines for $t = 1.7$ (-0.5 ± 0.1 and -0.7 ± 0.1 mag d^{-1} for STD and MU, respectively), and the value obtained from the public data at $t = 2.0$ d ($a_{\mathrm{ZTF},r} = -0.5 \pm 0.1$ mag d^{-1}). This example shows the benefit of advanced measurements (+16 h first estimation, and 40 h confirmation) during the rising phase of the transient, and this will be useful for any decision on spectroscopy observations before night-time in the Americas. This depends on our capacity to promptly analyse the data as soon as it is acquired. A two-day long rise in the r' band is atypical for standard KNe at 38 Mpc and could only be related to very particular ejecta configurations during an NS-BH collision (Bulla 2019). Also, we note an independent spectroscopic
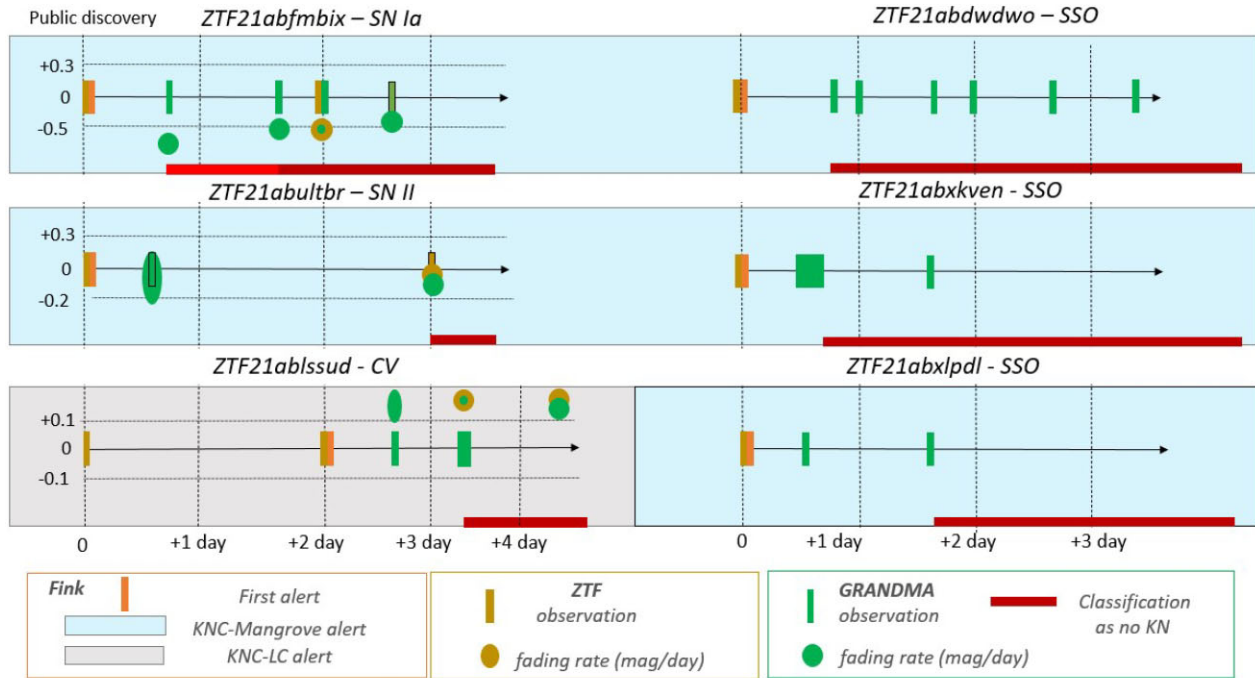
Figure 8. Overview of the GRANDMA observations of the six ZTF-Finkalerts followed up by professional and amateurs astronomers. The ZTF-Finkalerts came from two selection filters of the initial ZTF flux measurements named 'KN-LC' and 'KN-Mangrove' (see Section 3). Displayed in orange are the time-stamps for the first alert provided by FINK Gold vertical bars represent the time-stamps of the release of ZTF public data, and green vertical bars represent the GRANDMA data analysed by STDPIPE and MUPHOTEN. The circles present our fading slope estimation using r'/R filters (see Section 4.3); in gold using only ZTF public data, and in green using ZTF + GRANDMA data. Horizontal red bars show the period when the alert is considered as of no further interest for KN searches. SSO corresponds to Solar System Object, CV to cataclysmic variable, and SN to supernova given by our post-observation analysis months after (see fig. 4.4.4). We see the potential of the amateur community to distinguish astrophysical events into three categories: moving objects, fast transients (KNe, GRBs) and slow transients (supernovae, CVs).

measurement by the ZTF Spectral Energy Distribution Machine (SEDM) on $T_0 + 0.1$ d, classifying the source as a supernova Ia SNIascore (2021).

ZTF21abultbr was observed by three amateur telescopes and by the Abastumani-T70, providing a total of eight images from 0.6 to 2.5 d after T_0 (2021 August 21 02:44:39.100 UTC). The associated alert was sent by FINK with a 10 min latency with respect to the public detection. The source was presumably associated with UGC04104, located at 89 Mpc. Three of the eight images, taken with two different telescopes, led to a positive detection of the object using the STDPIPE and MUPHOTEN pipelines. These images were taken with in R and G bands, and also with unfiltered observations. The next public ZTF measurement ($r' = 18.7$ mag) was delivered three days after the first detection of the source. We note the consistency of photometric measurements between STDPIPE and MUPHOTEN, except for images taken with no filter. At $t = 6.0$ d, the luminosity rate (see Section 4.3) exhibits the following slopes: $a_{STD, r}(t = 0.6) = -0.3 \pm 0.4$ mag d^{-1} and $a_{MU, r}(t = 0.6) = -0.0 \pm 0.4$ mag d^{-1}. The value obtained from the public data at $t = 3.0$ d ($a_{ZTF,r'}(t = 3.0) = -0.0 \pm 0.1$ mag d^{-1}). These measurements were insufficient to conclude the nature of the transient and how it evolved from 0.6 to 3.0 d. The monitoring of the source by ZTF was interrupted between $t = 3.0$ to $t = 21.0$ d. The source was independently classified as a supernova II after 21 d by the ZTF SEDM Chu, Dahiwale & Fremling (2021).

ZTF21abxkven was observed simultaneously by the Abastunami/T70, TRT-SRO, Lisnyky/Schmidt-Cassegrain, and FRAM-CTA telescopes, as well as nine different amateur telescopes with a total of 17 images taken between 0.5 and 11.7 d after T_0

(2021 September 3 08:28:07). It was presumably associated with UGC12816 located at 80 Mpc based on the KN-Mangrove filter. The associated alert was sent by FINK without any further delay. With no more alert data sent for this location on the sky, FINK classified this transient independently as a Solar System object (Möller et al. 2020). All images resulted in non-detections with a median upper limit of 20.6 mag in unfiltered images within the first day of observation. A clear image (no filter) was taken at 0.7 d after T_0 by T-STSOPHIE, with a 20.6 mag upper limit. In summary, the GRANDMA follow-up ruled out any possible existing KN within 80 Mpc at $T_0 + 0.7$ d.

ZTF21abxlpdl was observed simultaneously by the Abastunami/T70, FRAM-CTA, and TRT-SRO telescopes, as well as seven amateur telescopes. A total of 15 images were taken from 0.5 to 13.9 d after the first public detection (2021 September 3 08:59:15). The alert was sent the same day as ZTF21abxkven, so the participation was limited for both targets. The transient was presumably associated with NGC 105, located at 79 Mpc based on our KN-Mangrove filter. The associated alert was sent by FINK without any further delay. All images resulted in non-detections with a median upper limit of 20.0 in unfiltered observations (see some examples in Table B1). A clear image was taken 1.7 d after the alert using the T40-A77DAU, with an upper limit estimated at >20.7 mag. In summary, the GRANDMA follow-up ruled out any KN within 80 Mpc at $T_0 + 1.7$ d with luminosity decay rate >1 mag d^{-1} in the r' band. Some scenarios involving both BNS and NSBH collisions can produce steeper decay rates >1 mag d^{-1} in the r' band, although these cases are extremely rare (see Bulla 2019).
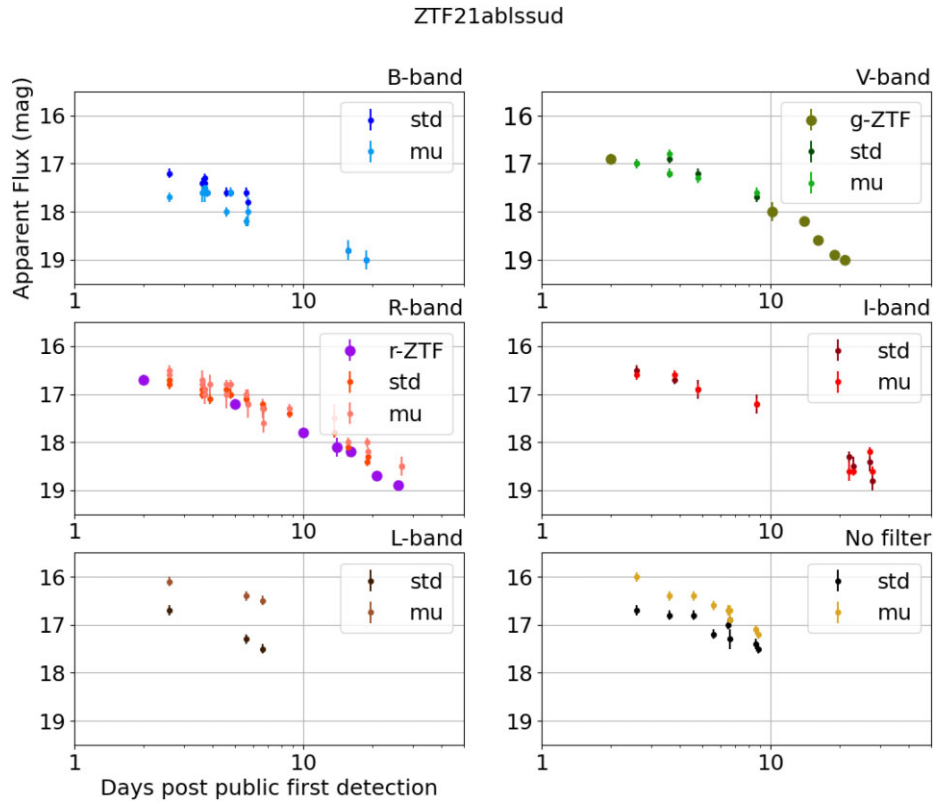
Figure 9. ZTF21ablssud light curves with ZTF as well as the GRANDMA observations from 17 different telescopes. The data were mostly taken by amateur astronomers before $t = T_0 + 10$ d, and by professionals for $t > T_0 + 10$ d. STDPIPE and MUPHOTEN measurements are in agreements for V, R_C, and I_C bands. In the L filter as well as in unfiltered images, MUPHOTEN adds flux from g'- and r'-band Pan-STARRS images while STDPipe treats them as R_C-band images. We show that the GRANDMA measurements are consistent with the ZTF ones, allowing for filling in the light-curve gaps. However the use of non-standard filters by some amateur astronomers (especially the B band of the T-CAT instrument) can lead to discrepancies between measurements up to 0.5 mag.

4.4.2 KN-LC alert candidates

ZTF21ablssud was observed simultaneously by the TRT-SRO, Lisnyky/Schmidt-Cassegrain, Tibet-50, and UBAI-NT60 telescopes, as well as 17 different amateur telescopes, leading to a total of 141 images taken between 2.6 and 26.7 d after T_0 (2021 July 16 21:11:45). The associated alert from the KN-LC filter was sent by FINK two days after the discovery with a probability of 53 per cent classification (see Section 3.2.1). Other classifications were delivered by FINK Early SN (5 per cent), Supernova SN Ia versus non-IA SN (73 per cent) and SN Ia and Core-Collapse versus non-SN (39 per cent). Observations started 0.6 d after the FINK alert. A total of 66 images taken with eight different filters (and additional unfiltered images) from 17 telescopes exhibited a positive detection of the object using both the STDPIPE and MUPHOTEN pipelines. The next public ZTF measurement post-FINK alert ($r' = 17.2$ mag in the r' band) was delivered five days after the first detection. For $t = 3.7$ d, we derived the slope of the luminosity decay rate (Section 4.3) as 0.15 ± 0.1 mag/day for both STDPIPE and MUPHOTEN. The slopes obtained from the ZTF public data are $a_{\mathrm{ZTF},\,r} = 0.15 \pm 0.1$ mag d^{-1} at $t = 2.0$ d and $t = 5.0$ d. We ruled out the association with a standard KN resulting from the coalescence of two binary neutron stars. No spectra have been reported in the literature. FINK scored the transient as Supernova (79 per cent) after 30 d of observations by ZTF. GRANDMA accumulated an important collection of data for $t < 10$ d compared to the available data in the literature (see Fig. 9). Based on the colour evolution and the location of the source close to the galactic plane, we proposed that the source corresponds to a cataclysmic variable event. In

addition, the light-curve fitting of ZTF data ruled out the nature of the source as a KN, GRB afterglow, or supernova event (see Section 4.4.4).

4.4.3 Training alert candidates

Here, we briefly describe our observations on 'training alerts' distributed by FINK. The alerts are produced via different channels: supernova and KN candidates. They were only scheduled for Fridays and were proposed for observing on a best-effort basis by the FINK team for practice.

ZTF21abfaohe/SN 2021pfs and ZTF21abbzjeq/ SN 2021mwb were classified as supernovae (see TNS for external reference and Section 4.4.4). ZTF21abotose/SN 2021ugl is a supernova IIb. The three sources distributed via FINK were selected to test the data reduction capabilities of GRANDMA. Photometric results are reported in Appendix B.

ZTF21abyplur was only observed by the Tibet-50 with four images beginning 9.5 d after the first public detection reported on 2021 September 7 09:12:26. The associated alert was sent by FINK without any further delay but the amateur astronomers were not notified because it was outside of our Friday exercise. The alert-host association (PGC1115282) is within 10 arcsec, almost at the limit of a positive association; it might have been incorrectly associated with the galaxy. FINK classified this object independently as a Solar System object, probably attached to Solar System object number 22327 (Möller et al. 2020). The images taken by the Tibet-50 could

Table 3. Results of the simulations of transients with rapid evolution, in order to validate or reject the concordance of each transient using ZTF data with the four models: KNe (Ka2017), supernova (nugent-hyper), GRB afterglows (TrPi2018), and shock cooling (Piro2021). Note that the Bayes factors are evaluated logarithmically.

Transients	Ka2017	TrPi2018	nugent-hyper	Piro2021	light curve
ZTF21abfmbix	−12.38	−15.95	−9.18	−10.1	Supernova Ia
ZTF21absvlrr	−9.78	−16.73	−9.91	−11.07	Supernova Ia
ZTF21abultbr	−2.73	-9.14	−5.24	−4.76	Supernova II
ZTF21ablssud	−6.32	−11.58	−9.83	−9.41	Cataclysmic Variable
ZTF21abfaohe	−12.3	−10.98	−7.47	8.67	Supernova Ia
ZTF21abbzjeq	−8.22	−11.41	−7.49	−8.47	Supernova Ia
ZTF21acceboj	−16.52	−19.44	−14.52	−15.6	Supernova IIb
ZTF21abotose	−6.37	−10.62	−7.41	−7.49	Shock Cooling - Supernova IIp

not rule out the case of a fast transient with an upper limit of $g' > 18.3$ mag, at $t = T_0 + 9.5$ d.

ZTF21absvlrr was observed by six amateur telescopes and the Terskol/Zeiss-600, TRT-SBO, TRT-SRO, and Abastumani-T70 telescopes, leading to a total of 24 images taken from 1 to 59 d after T_0 (2021 August 12 09:52:43). The associated alert from the KN-Mangrove filter was sent by FINK with a 2.3 h delay, but distributed to GRANDMA as a practical exercise about 0.9 d afterwards. The source was presumably associated with ESO540-025 located at 89 Mpc. A total of 19 images taken with seven telescopes confirmed a positive detection of the source using both STDPIPE and MUPHOTEN pipelines. These images were taken in B, V, r', R, as well as unfiltered. The next public ZTF measurement ($g' = 17.6$ mag, $r' = 17.7$ mag) was delivered two days after the first detection. We note the consistency of photometric measurements between STDPIPE and MUPHOTEN, except for images taken with no filter. According to the results obtained with both pipelines, the data clearly shows a transient in the rising phase in the r' band, based on the slopes of the light curves at $t = 1.0$ d (-0.1 ± 0.2 mag d^{-1} for both STD and MU), and at $t = 1.7$ d (-0.5 ± 0.1 and -0.7 ± 0.1 mag d^{-1} for STD and MU, respectively). At $t = 2.0$ d, the slope obtained from the ZTF public data is $a_{\mathrm{ZTF, r}} = -0.5 \pm 0.1$ mag d^{-1}. In addition, we also observed a two-day long rise of the source in B (-0.7 ± 0.2 and -0.8 ± 0.2 mag d^{-1} for STD and MU, respectively, at $t = 2.0$ d) and in the g'-band ($a_{\mathrm{ZTF; g}}(t = 2.0) = -0.6 \pm 0.1$ mag d^{-1}). The source, at an early stage, did not behave in a manner similar to AT2017gfo. We note an independent spectroscopic measurement by the ZTF SEDM on $T_0 + 1$ d, classifying the source as a supernova IaRidley et al. (2021).

ZTF21acceboj/SN 2021yyg was only observed by Tibet-50 and Terskol-600 telescopes with a total of 11 images taken after 1.4 d from the first public detection reported on 2021 September 14 11:04:25. The associated alert from the KN-Mangrove filter was sent by FINK without any further delay but the amateur astronomers were not notified since it was out of our Friday triggering schedule. From linear regression fitting (see Section 4.3) we obtained $a_{\mathrm{STD, r}}(t = 1.4) = -0.3 \pm 0.1$ mag d^{-1}, and $a_{\mathrm{MU, r}}(t = 1.4) = -0.4 \pm 0.1$ mag d^{-1}. Using public data we measured $a_{\mathrm{ZTF, r}}(t = 2.0) = -0.3 \pm 0.1$ mag d^{-1}. The source clearly exhibits a two-day rise in the r' band that ruled out ZTF21acceboj as a KN stemming from the coalescence of two binary neutron stars. The Global SN Project (with LCO) classified the source as a supernova IIp one day after than the first public detection Burke et al. (2021).

4.4.4 Constraining the nature of transients with offline results

The objective of the 'ReadyforO4' campaign was to gather information on the nature of transient events and their evolution. Events were

followed during weekends, but not monitored over several weeks. Hence our GRANDMA sample covered essentially two epochs: when the alert was received by our amateur astronomers, and when the professional telescopes joined the campaign in July. In this sense, we trained our team on the ZTF data available to confirm the nature of the sources we followed up with GRANDMA using models described in Section 4.3. The ZTF data are used to validate the models by generating the logarithm of the Bayes factor, the level of correlation of the model fit with the data, and increase our knowledge of the physical processes following the observation.

In Table 3, we present the results obtained for each transient clearly identified as a non-moving object through the analysis of the light curve from ZTF data. While the best-fitting light-curve models varied, including some preferring a kilonova origin at early times, the relative parity between the Bayes factors mostly indicated insufficient information, especially at early times, to differentiate between models. This motivates GRANDMA's goals of augmenting early time photometry to better differentiate and prioritize objects. We identified ZTF21abfmbix, ZTF21absvlrr, ZTF21abultbr, ZTF21abfaohe, ZTF21abfmbix, ZTF21abbzjeq, and ZTF21acceboj as typical supernova candidates. ZTF21abotose is both consistent with shock cooling and GRB afterglow models at early times. However, the increase of its brightness at later times is in good agreement with the shock cooling scenario only. ZTF21ablssud is well-fit by a GRB model, however, due to its galactic latitude ($\ell = 5.7$ deg) and similarity to many other examples of cataclysmic variables in the literature, it is likely a cataclysmic variable.

5 CONCLUSIONS

In this paper we describe GRANDMA's 'ReadyforO4' campaign to search for serendipitous KNe using ZTF public data filtered by FINK and followed-up with GRANDMA facilities. Eight objects in total were observed, using 26 amateur telescopes and eleven professional telescopes (34 of which provided data analysed in this work). Through FINK and follow-up, no KNe were identified, instead we classified four of these objects as asteroids, while the remaining were classified as cataclysmic variables and supernovae. In addition to demonstrating a number of challenges for observing transient sources with a variety of telescopes of different apertures, filters, and configurations, we achieved a number of successes.

(i) **Reaction time** – We obtained the first images from the amateur community less than 16 h after the FINK alert. This delay is due to the fact that most of our amateur community is located in Europe (especially in France). In the future we hope to connect with other amateurs across the world, although language barriers remain a challenge.

(ii) **Data acquisition and filters** – The GRANDMA facilities are mostly equipped with red filters, which are excellent for the characterization of KNe events. Our campaign showed that amateur astronomers reached a depth of 21 mag with a variety of filter configurations. These astronomers will be an asset during O4, for which we might expect AT2017gfo-type KN events peaking at ∼21 mag for events located at the observational horizon of the GW interferometers (Petrov et al. 2022). However, the use of filter sets (Johnson-Cousins, *L*-, *w*- and *o*-filters) different from those of the SDSS, which was our reference catalogue for this analysis, remains problematic for the characterization of the sources. For this reason, we found that the use of two standard data reduction pipelines (STDPIPE and MUPHOTEN) is a way to standardize results (as compared to allowing the individual telescope teams to reduce their own data). We observed a difference in magnitude of less than 0.2 mag for Johnson-Cousins and SDSS filters. Based on this experience, we would like to motivate our community to use only SDSS filters to have a homogeneous set of data. We also noted that images taken with no filter are particularly useful for guiding the observers for their data acquisition. We finally experienced miscommunication on products distributed to GRANDMA, as some observers provided pre-stacked images while others were submitted as individual images. This greatly reduced our ability to analyse the images at low latency, and so correcting this will be a focus for future campaigns.

(iii) **Quality of the data sample** – Among the eight transients, a total of 450 images were taken by GRANDMA partners. However, we detected a source and were able to perform astrometry and photometry on only 180 images (40 per cent). To improve this efficiency, we need amateur astronomers to gain expertise in their data acquisition and validation before distribution to the network. For example, some data had artifacts and 'star' tracks, blur, or galaxy saturation that could easily be identified with more experience. Another challenge was the dispersion of format and keywords employed in the files, which slowed down our analysis. This will be partially solved in future runs with a set of required keywords, including the time of the start of the observation, the name of the telescope, the filter used and the filter system.

(iv) **Classification** – We demonstrated the potential of the amateur community to distinguish astrophysical events into three categories: moving objects, fast transients (KNe, GRBs), and slow transients (supernovae, CVs). We based our rapid fast transient classification on the decay rate of the optical sources, which should reach a maximum of at least 0.3 mag d^{-1} for KNe. The images posted by the professional and amateurs observers within the first 2 d after the FINK alert helped to categorize the candidates, which were discovered at an average magnitude of r' 18.1 ± 1.0 mag. This classification improved on the timing relative to routine observations by ZTF during the American night. In addition, we also developed rapid and sophisticated modelling tools that can be applied to GRANDMA data during the O4 observing run. If we are able to run data reduction in near real-time, we would be able to filter the most probable candidates a few hours before the second night of observation in the Americas after a GW alerts. This will allow us to trigger spectroscopic observations with higher confidence during the O4 observing run, mitigating the use of valuable resources on non-viable candidates.

Overall, we consider the first 'ReadyforO4' campaign to be a success which can be built upon to allow the amateur community to partake in cutting-edge astrophysical science once the fourth observing run of the LIGO-Virgo-KAGRA detectors begins in late 2022/early 2023.

DATA AVAILABILITY

The data underlying this article will be shared on reasonable request to the corresponding author.

REFERENCES

Abbott B. P. et al., 2017a, Phys. Rev. Lett., 119, 161101
Abbott B. P. et al., 2017b, ApJ, 848, L12
Alexander K. D. et al., 2017, ApJ, 848, L21
Almualla M. et al., 2021, MNRAS, 504, 2822
Almualla M., Coughlin M. W., Anand S., Alqassimi K., Guessoum N., Singer L. P., 2020, MNRAS, 495, 4366
Andreoni I. et al., 2019, PASP, 131, 068004

Andreoni I. et al., 2022, ApJS, 258, 5
Andreoni I. et al., 2021, ApJ, 918, 63
Andreoni I. et al., 2017, Publ. Astron. Soc. Austr., 34, e069
Antier S. et al., 2020a, MNRAS, 492, 3904
Antier S. et al., 2020b, MNRAS, 497, 5518
Arcavi I. et al., 2017, Nature, 551, 210
Barbary K., 2016, J. Open Source Softw., 1, 58
Bauswein A., Just O., Janka H.-T., Stergioulas N., 2017, ApJ, 850, L34
Becker A., 2015, HOTPANTS: High Order Transform of PSF ANd Template Subtraction, record ascl:1504.004
Bellm E. C. et al., 2019, PASP, 131, 068003
Berger E., 2014, Ann. Rev. Astron. Astrophys., 52, 43
Berger E., Fong W., Chornock R., 2013, ApJ, 774, L23
Bertin E., 2006, in Gabriel C., Arviset C., Ponz D., Solano E., eds, ASP Conf. Ser. Vol. 351, Automatic Astrometric and Photometric Calibration with SCAMP. Astron. Soc. Pac., San Francisco, p. 112
Bertin E., 2011a, in Evans I. N., Accomazzi A., Mink D. J., Rots A. H., eds, ASP Conf. Ser. Vol. 442, Astronomical Data Analysis Software and Systems XX. Astron. Soc. Pac., San Francisco, p. 435
Bertin E., 2011b, in Evans I. N., Accomazzi A., Mink D. J., Rots A. H., eds, ASP Conf. Ser. Vol. 442, Automated Morphometry with SEextractor and PSFEx. Astron. Soc. Pac., San Francisco, p. 435
Bertin E., Arnouts S., 1996, A&AS, 117, 393
Bertin E., Mellier Y., Radovich M., Missonnier G., Didelon P., Morin B., 2002, in Bohlender D. A., Durand D., Handley T. H., eds, ASP Conf. Ser. Vol. 281, Astronomical Data Analysis Software and Systems XI. Astron. Soc. Pac., San Francisco, p. 228
Bloemen S., Groot P., Nelemans G., Klein-Wolt M., 2015, in Rucinski S. M., Torres G., Zejda M., eds, Astronomical Society of the Pacific Conference Series Vol. 496, Living Together: Planets, Host Stars and Binaries. Astron. Soc. Pac., San Francisco, p. 254
Boch T., Fernique P., Bonnarel F., Chaitra C., Bot C., Pineau F. X., Baumann M., Michel L., 2020, in Pizzo R., Deul E. R., Mol J. D., de Plaa J., Verkouter H., eds, ASP Conf. Ser. Vol. 527, Astronomical Data Analysis Software and Systems XXIX. Astron. Soc. Pac., San Francisco, p. 121
Bradley L. et al., 2021, astropy/photutils: 1.1.0
Brennan S. J., Fraser M., 2022, preprint (arXiv:2201.02635)
Bulla M., 2019, MNRAS, 489, 5037
Burke J., Hiramatsu D., Howell D. A., McCully C., Newsome M., Gonzalez E. P., Pellegrino C., 2021, Transient Name Server Classification Report, 2021-3199, 1
Chornock R. et al., 2017, ApJ, 848, L19
Chu M., Dahiwale A., Fremling C., 2021, Transient Name Server Classification Report, 2021-3134, 1
Coughlin M. W. et al., 2018, MNRAS, 480, 3871
Coughlin M. W. et al., 2020a, Phys. Rev. Res., 2, 022006
Coughlin M. W. et al., 2020b, Nat. Commun., 11, 4129
Coughlin M. W. et al., 2020c, MNRAS, 492, 863
Coughlin M. W. et al., 2020d, MNRAS, 497, 1181
Coughlin M. W., Dietrich T., Margalit B., Metzger B. D., 2019, MNRAS, 489, L91
Coulter D. A. et al., 2017, Science, 358, 1556
Cowperthwaite P. S. et al., 2017, ApJ, 848, L17
Cowperthwaite P. S., Villar V. A., Scolnic D. M., Berger E., 2019, ApJ, 874, 88
Dekany R. et al., 2020, PASP, 132, 038001
Dietrich T., Coughlin M. W., Pang P. T. H., Bulla M., Heinzel J., Issa L., Tews I., Antier S., 2020, Science, 370, 1450
Dokkum (van) P. G., 2001, PASP, 113, 1420
Ducoin J.-G., Corre D., Leroy N., LeÂFloch E., 2020, MNRAS, 492, 4768
Duev D. A. et al., 2019, MNRAS, 489, 3582
Duverne P. A. et al., 2022, MUPHOTEN: a MUlti-band PHOtometry Tool for TElescope Network, preprint (arXiv:2201.07565)
Flaugher B. et al., 2015, AJ, 150, 150
Ginsburg A. et al., 2019, AJ, 157, 98
Goldstein A. et al., 2017, ApJ, 848, L14
Gompertz B. P. et al., 2020, MNRAS, 497, 726–738
Graham M. J. et al., 2019, PASP, 131, 078001

Haggard D., Nynka M., Ruan J. J., Kalogera V., Cenko S. B., Evans P., Kennea J. A., 2017, ApJ, 848, L25
Hallinan G. et al., 2017, Science, 358, 1579
Hotokezaka K., Nakar E., Gottlieb O., Nissanke S., Masuda K., Hallinan G., Mooley K. P., Deller A. T., 2019, Nat. Astron., 3, 940
Ho A. Y. Q. et al., 2022, preprint (arXiv:2201.12366)
Hu L. et al., 2017, Sci. Bull., 62, 1433
Ivezić Ž. et al., 2019, ApJ, 873, 111
Karpov S., 2021, STDPipe: Simple Transient Detection Pipeline, record ascl:2112.006
Kasen D., Metzger B., Barnes J., Quataert E., Ramirez-Ruiz E., 2017, Nature, 551, 80
Kasliwal M. M. et al., 2020, ApJ, 905, 145
Kostov A., Bonev T., 2018, Bulg. Astron. J., 28, 3
Lang D., Hogg D. W., Mierle K., Blanton M., Roweis S., 2010, AJ, 139, 1782
Levan A. et al., 2005, ApJ, 624, 880
Margalit B., Metzger B. D., 2017, ApJ, 850, L19
Margutti R. et al., 2018, Target of Opportunity Observations of Gravitational Wave Events with LSST, recordarXiv:1812.04051
Masci F. J. et al., 2019, PASP, 131, 018003
McCully C., Tewes M., 2019, Astro-SCRAPPY: Speedy Cosmic Ray Annihilation Package in Python, record ascl:1907.032
Möller A. et al., 2020, MNRAS, 501, 3272
Morgan J. S., Kaiser N., Moreau V., Anderson D., Burgett W., 2012, in Stepp L. M., Gilmozzi R., Hall H. J., eds, Proc. SPIE Conf. Ser. Vol. 8444, Ground-based and Airborne Telescopes IV. SPIE, Bellingham, p. 84440H
Patterson M. T. et al., 2019, PASP, 131, 018001
Perley D. A. et al., 2019, MNRAS, 484, 1031
Petrov P. et al., 2022, ApJ, 924, 54
Piro A. L., Haynie A., Yao Y., 2021, ApJ, 909, 209
Ridley E., Gompertz B., Nicholl M., Galbany L., Yaron O., 2021, Transient Name Server Classification Report, 2021-2795, 1
Savchenko V. et al., 2017, ApJ, 848, L15
SNIascore, 2021, Transient Name Server Classification Report, 2021-2021, 1
Tachibana Y., Miller A. A., 2018, PASP, 130, 128001
Tanvir N. R., Levan A. J., Fruchter A. S., Hjorth J., Hounsell R. A., Wiersema K., Tunnicliffe R. L., 2013, Nature, 500, 547
Tonry J. L. et al., 2018, PASP, 130, 064505
Troja E. et al., 2018, MNRAS, 478, L18
Waters C. Z. et al., 2020, ApJS, 251, 4

SUPPORTING INFORMATION

Supplementary data are available at *MNRAS* online.

MN-22-0618-MJ.R2_suppmaterial.pdf
APPENDIX A: LINEAR FITTING REGRESSION
APPENDIX B: OBSERVATIONS FROM THE GRANDMA PROGRAM
Table B1. Upper limits - Summary of the GRANDMA observations of some KN-MANGROVE alerts.
Table B2. Detections - Summary of the GRANDMA observations of ZTF-Fink candidates.

Please note: Oxford University Press is not responsible for the content or functionality of any supporting materials supplied by the authors. Any queries (other than missing material) should be directed to the corresponding author for the article.

[1]*E. Kharadze Georgian National Astrophysical Observatory, Mt. Kanobili, Abastumani, Adigeni 0301, Georgia; Ilia State University, Kakutsa Cholokashvili ave 3/5, Tbilisi 0162, Georgia*

[2]*Samtskhe-Javakheti State University, Rustaveli Str. 113, Akhaltsikhe 0080, Georgia*

[3]*American University of Sharjah, Physics Department, PO Box 26666 Sharjah, UAE*

[4]*Artemis, Observatoire de la Côte d'Azur, Université Côte d'Azur, Boulevard de l'Observatoire, F-06304 Nice, France*

[5]*GRAPPA, Anton Pannekoek Institute for Astronomy and Institute of High-Energy Physics, University of Amsterdam, Science Park 904, NL-1098 XH Amsterdam, the Netherlands*

[6]*Université de Paris, CNRS, Astroparticule et Cosmologie, F-75013 Paris, France*

[7]*Astronomical Observatory Taras Shevshenko National University of Kyiv, Observatorna str. 3, UA-04053 Kyiv, Ukraine*

[8]*Physics Department, University of Iceland, Sæmundargata 2, 102 Reykjavík, Iceland*

[9]*Aix Marseille Univ, CNRS, CNES, LAM, IPhU, F-13007 Marseille, France*

[10]*Société Astronomique de Lyon, 9 Avenue Charles André, F-69230 Saint Genis Laval, France*

[11]*ICAMER Observatory of NAS of Ukraine 27 Acad. Zabolotnoho Str., UA-03143 Kyiv, Ukraine*

[12]*Instituto de Astrofísica de Andalucía (IAA-CSIC), Glorieta de la Astronomía s/n, E-18008 Granada, Spain*

[13]*Université Grenoble-Alpes, Université Savoie Mont Blanc, CNRS/IN2P3 Laboratoire d'Annecy-le-Vieux de Physique des particules, F-74940, France*

[14]*Observatoire de Dauban, 04 Banon - F-13010, France*

[15]*Groupe Astronomique de Querqueville, 61, rue Roger Glinel, F-50460 Cherbourg en cotentin, France*

[16]*Vereniging Voor Sterrenkunde, Balen-Neetlaan 18A, B-2400 Mol, Belgium*

[17]*Zeeweg 96, B-8200 Brugge, Belgium*

[18]*Ulugh Beg Astronomical Institute, Uzbekistan Academy of Sciences, Astronomy str. 33, Tashkent 100052, Uzbekistan*

[19]*MP-G2A, Midi Pyrénées, Groud Astrophysic Addict, F-81570 Cuq, France*

[20]*El Center for Backyard Astrophysics, New York, NY 10027, USA*

[21]*School of Physics and Astronomy, University of Minnesota, Minneapolis, MN 55455, USA*

[22]*Institute for Physics and Astronomy, University of Potsdam, D-14476 Potsdam, Germany*

[23]*Max Planck Institute for Gravitational Physics (Albert Einstein Institute), Am Mühlenberg 1, D-14476 Postsdam, Germany*

[24]*OHP, Observatoire de Haute-Provence, CNRS, Aix Marseille University, Institut Pythéas, St Michel l'Observatoire, F-04870, France*

[25]*IJCLab, Univ Paris-Saclay, CNRS/IN2P3, F-91400Orsay, France*

[26]*Institut d'Astrophysique de Paris, 98 bis boulevard Arago, F-75014 Paris France*

[27]*Institute of Earth Systems, University of Malta, MSD 2080, Malta*

[28]*Znith Observatory, 1018 Naxxar, Malta*

[29]*APPAM, F-81360 Montredon-Labessonnié, France*

[30]*Department of Chemical and Physical Sciences, The University of the Virgin Islands, US-VI 00802, USA*

[31]*Volkssternwarte Paderborn, Im Schloßpark 13, D-33104 Paderborn, Germany*

[32]*Hidden Valley Observatory, E9891 810th Ave., Colfax, WI E9891, USA*

[33]*LPC, Université Clermont Auvergne, CNES/IN2P3, F-63170 Aubière, France*

[34]*Dunedin Astronomical Society (DAS), 1A City Road, Robin Hood Park, 9059 Dunedin, New Zealand*

[35]*FZU - Institute of Physics of the Czech Academy of Sciences, Na Slovance 1999/2, CZ-182 21 Praha, Czech Republic*

[36]*Laboratoire de Physique et de Chimie de l'Environnement, Université Joseph KI-ZERBO, 03 BP 7021 49 - 44-105, Ouagadougou, Burkina Faso*

[37]*IRAP, Université de Toulouse, CNRS, UPS, 14 Avenue Edouard Belin, F-31400 Toulouse, France*

[38]*Université Paul Sabatier Toulouse III, Université de Toulouse, 118 route de Narbonne, F-31400 Toulouse, France*

[39]*Contern Observatory, L-5316 Contern, Luxembourg*

[40]*Beijing Planetarium, Beijing Academy of Science and Technology, Beijing 100044, China*

[41]*Montarrenti Observatory, S.S. 73 Ponente, I-53018 Soviville, Siena, Italy*

[42]*OPERA Z97-, F-33820 Saint Palais, France*

[43]*Observatory Uranoscope de l'Ile de France, Allee Camille Flammarion, F-77220 Gretz -Armainvilliers, France*

[44]*Observatoire du 'Crous des Gats', F-31550 Cintegabelle, France*

[45]*Centre for Astrophysics and Supercomputing, Swinburne University of Technology, Mail Number H29, PO Box 218, 31122 Hawthorn, VIC, Australia*

[46]*OAR Telescope/NSF's NOIRLab, Avda Juan Cisternas 1500, 1700000 La Serena, Chile*

[47]*National Astronomical Research Institute of Thailand (Public Organization), 260, Moo 4, T. Donkaew, A. Mae Rim, Chiang Mai 50180, Thailand*

[48]*OrangeWave Innovative Science, LLC, Moncks Corner, SC 29461, USA*

[49]*Department of Electronics, Electrical Engineering and Microelectronics, Silesian University of Technology, Gliwice, Poland*

[50]*Université de Strasbourg, CNRS, IPHC UMR 7178, F-67000 Strasbourg, France*

[51]*School of Physics and Astronomy, Rochester Institute of Technology, 84 Lomb Memorial Drive, Rochester, NY 14623, USA*

[52]*Main Astronomical Observatory of National Academy of Sciences of Ukraine, 27 Acad. Zabolotnoho Str., UA-03143 Kyiv, Ukraine*

[53]*Société Astronomique Populaire du Centre, 40 grande rue, F-18340 Arçay, France*

[54]*Université Paris-Saclay, Université Paris Cité, CEA, CNRS, AIM, F-91191 Gif-sur-Yvette, France*

[55]*Astronomy and Space Physics Department, Taras Shevchenko National University of Kyiv, Glushkova ave., 4, UA-03022 Kyiv , Ukraine*

[56]*National Center, Junior academy of sciences of Ukraine, 38-44, Dehtiarivska St., UA-04119 Kyiv, Ukraine*

[57]*Institute of Gravitational Research, University of Glasgow, Glasgow G12 8QQ, Scotland*

[58]*ICAstronomy, Oria, E-04810 Almería, Spain*

[59]*Deep Sky Chile, Pichasca, Rio Hurtado 1870000, Chile*

[60]*National University of Uzbekistan, 4 University str., Tashkent 100174, Uzbekistan*

[61]*INFN, Laboratori Nazionali del Sud, I-95125 Catania, Italy*

[62]*Physics Department and Tsinghua Center for Astrophysics, Beijing 100084, China*

This paper has been typeset from a TEX/LATEX file prepared by the author.